Porphyrin-xylan-coated silica nanoparticles for anticancer photodynamic therapy

Soukaina Bouramtane, Ludovic Bretin, Aline Pinon, David Leger, Bertrand Liagre, Laurence Richard, Frédérique Brégier, Vincent Sol, Vincent Chaleix

Porphyrin-xylan-coated silica nanoparticles for anticancer photodynamic therapy

Soukaina Bouramtane[a], Ludovic Bretin[b], Aline Pinon[b], David Leger[b], Bertrand Liagre[b], Laurence Richard[c], Frédérique Brégier[a], Vincent Sol[a], Vincent Chaleix[a, *]

[a] Université de Limoges, Laboratoire PEIRENE, EA 7500, Faculté des Sciences et Techniques, 123 Avenue Albert Thomas, 87060 Limoges, France.

[b] Université de Limoges, Laboratoire PEIRENE EA 7500, Faculté de Pharmacie, – 2, rue du Docteur Marcland, 87025 Limoges, France.

[c] Centre Hospitalier Universitaire de Limoges, Service d'Anatomie Pathologique – 2, avenue Martin Luther King 87042 Limoges cedex, France.

∗ Corresponding author. Tel.: +33 05 55 45 75 67; Fax: +33 05 55 45 72 02. E-mail address: vincent.chaleix@unilim.fr (V. Chaleix).

Highlights

- Xylan-porphyrin-coated silica nanoparticles (PX SNPs) have been synthesized.
- Valorization of hemicellulose as a drug carrier for photodynamic therapy.
- Formed nanoparticles show high anticancer activity against colorectal cancer cell lines.

Abstract

Porphyrins are widely used in anticancer photodynamic therapy (PDT). However, low physiological solubility and lack of selectivity towards cancer cells are the main limitations of their clinical use. Nanoparticles are being intensively explored as photosensitizer carriers for PDT to overcome these limitations. The aims of this work are to synthesize core-shell hybrid nanoparticles formed by a silica core and xylan carrying a 5-(4-hydroxyphenyl)-10,15,20-triphenylporphyrin (TPPOH) shell, and evaluate their anticancer activity. To afford drug-controlled incorporation and enhance blood circulation, TPPOH was covalently linked to xylan. Different xylans with degrees of substitution in TPPOH ranging from 0.034 to 1.11, were obtained and characterized. Then, the xylan-TPPOH conjugate (PX) was used to coat the silica nanoparticles (PX SNPs). The obtained nano-objects were characterized and their therapeutic potential for photodynamic therapy evaluated against colorectal cancer cell lines.

In vitro analysis showed that PX SNPs were 40-fold and 10-fold more effective against HCT116 cells and HT-29 cells respectively compared to free TPPOH.

Keywords : xylan; polysaccharides; silica nanoparticles; photodynamic therapy; colorectal cancer.

1. Introduction

Being the second leading cause of death in the world, after cardiovascular pathologies, cancer is the most dreaded disease of our time (Nagai & Kim, 2017). It consists of the anarchic proliferation of abnormal cells which escape from normal control mechanisms. Several options are available for treating cancer; the most classic are surgery, chemotherapy and radiotherapy (Saini, Chouhan, Bagri, & Bajpai, 2012). These treatments are invasive and lack selectivity toward tumor cells. To better target cancer cells and minimize adverse effects, new or complementary treatments have emerged over the past few years.

Photodynamic therapy (PDT) is an alternative and non-invasive cancer treatment requiring the simultaneous presence of three elements: a photosensitive molecule, a light source and molecular oxygen (Kwiatkowski et al., 2018). PDT usually involves intravenous administration of a photosensitizer (PS) and subsequent specific-wavelength irradiation of the tumor tissue. When irradiated, the PS passes from the ground state to the excited singlet state. The excited photosensitizer is very unstable and loses its excess energy by, either non-radiative (heat emission) or radiative (fluorescence emission) pathways. Another process can occur, namely intersystem crossing, to form a more stable excited triplet state with parallel spins. In this case, return to the ground state, theoretically forbidden transition, is very slow. PS can be deactivated by phosphorescence or by reacting with its environment according to two types of mechanisms. The Type I mechanism involves electron transfer from photosensitizer to biological substrates to form radicals and radical ions which, after interaction with oxygen, provide reactive oxygen species (ROS) such as the superoxide radical anion ($O_2^{\bullet -}$). A Type II photochemical process consists of a triplet-triplet energy transfer from PS to molecular oxygen in its ground state (triplet state). This energy transfer leads to the formation of singlet oxygen $^1O_2$ and thus regenerates the ground-state photosensitizer. All these species are highly reactive and are very powerful oxidants that can damage cancer cells and lead to their death (Bonnett, 1995; Henderson & Dougherty, 1992). Tetrapyrrole compounds such as porphyrins, chlorins, and bacteriochlorins are the most utilized photosensitizers in PDT (Abrahamse & Hamblin, 2016; Sternberg, Dolphin, & Brückner, 1998). However, these hydrophobic molecules are sparingly soluble in biological fluids and they suffer from poor selectivity towards tumor cells which restricts their use in clinical protocols.

Several approaches have been developed to improve PS bioavailability and efficacy in PDT. One of the most promising is the attachment of PS to nanoparticles (NPs) (Kydd et al.,2017)

which not only enhances the solubility of hydrophobic photosensitizers but also promotes their deposition inside tumors, due to so-called passive targeting. Indeed, leaky vasculature and the resulting aberrant architecture of solid tumors leads to preferential nanoparticle accumulation in tumors which remain there because of poor lymphatic drainage. This phenomenon, known as Enhanced Permeability and Retention (EPR) effect, was first described by Matsumura and Maeda (Matsumura & Maeda, 1986; Maeda & Matsumura, 1989; Maeda, 2001).

Various NPs have been used as delivery systems for water-insoluble drugs (Debele, Peng, & Tsai, 2015), and especially silica nanoparticles (SNPs), which have been recognized as promising vectors for PDT applications (Bharathiraja et al., 2017; Brezániová et al., 2018; Roy et al., 2003; Yan & Kopelman, 2003; Yan et al., 2018;). In the last two decades, SNPs have gained an ever-increasing interest for medical applications because of a large number of qualities, including biocompatibility, stability, high specific surface area, ease of synthesis with controllable size, shape and surface charge, along with their ease of functionalization with a number of varied materials (Tamba et al., 2015).

A major obstacle to controlled drug delivery is the mononuclear phagocytic system (MPS) which is responsible for the premature removal of drug carriers from the body through opsonization (Frank & Fries, 1991; Gref et al., 1994). One solution proposed to slow opsonization and increase nanoparticle half-lives in the bloodstream by coating them with hydrophilic groups via adsorption or covalent grafting (Lemarchand, Gref, & Couvreur, 2004). These groups generally consist of long chain polymers such as polyethylene glycol (PEG) (Mozar & Chowdhury, 2018; Peracchia et al., 1999), or polysaccharides such as chitosan (Zhu et al., 2009) and dextran (Coombes et al., 1997; Mbakidi et al., 2013). These polymers create a hydrophilic protective layer around the nanoparticles which prevents the binding of opsonins via steric repulsion forces, thereby delaying opsonization and phagocytosis (Owens & Peppas, 2006).

Xylan is a natural, biodegradable, and non-toxic biomaterial. It is the main hemicellulose component of secondary cell walls constituting approximately 20–30% of the biomass of dicotyl plants (hardwoods and herbaceous plants). In hardwood, 4-*O*-methylglucuronoxylan (MGX) is the most abundant hemicellulose. Its structure consists of a β(1-4)-D-xylopyranosyl backbone with 4-*O*-methyl-D-glucuronic acid (MeGlcA) side chains attached at the 2 position of the xylose units (Ebringerová & Hromádková, 2005). The degree of substitution in MeGlcA depends on the forest species and varies between 3.7 and 12 xylose units for one 4-

O-methylglucuronic acid unit in hardwoods. Xylan obtained from corn cobs has been reported to exhibit antioxidant, anticoagulant, antimicrobial and antiproliferative properties. Corn cob xylan has been shown to exert an antiproliferative effect against HeLa cell lines in a dose-dependent manner (Melo-Silveira et al., 2012). In another study, chestnut tree MGX was found to inhibit proliferation of A431 human squamous carcinoma cells, as well as migration and invasion by inhibiting the expression of metalloproteinases MMP2 and MMP9, which are involved in the degradation of the cell basement membrane and subsequent migration through extracellular matrices (Moine et al., 2007). In drug delivery, esterification of beech wood xylan via activation of the carboxylic acid with N, N-carbonyldiimidazole has been performed to produce prodrugs for the controlled release of ibuprofen (Daus & Heinze, 2010). The surface modification of magnetic nanoparticles (MNPs) with xylan has also been reported to stabilize MNPs in biological media and been shown to improve their biocompatibility and biodistribution (Ma et al., 2018).

The functionalization of xylan by porphyrins has never been reported in the literature. We hypothesize that it should be possible to condense porphyrins on xylan by esterification and to control the degree of substitution through the implementation of a well-chosen experimental design. We assume that it must be possible to obtain nano-objects with high porphyrin content through surface coating of SNPs with PX conjugate. We also assume that the anticancer activity of these nanoparticles will be higher than that of free TPPOH.

In adequation with our research program on polysaccharide modifications with photosensitizers for PDT applications (Drogat et al., 2012; Ringot et al., 2018), and in order to develop new photosensitizer carriers for PDT applications, we prepared and characterized core-shell hybrid nanoparticles based on xylan for the targeted delivery of 5-(4-hydroxyphenyl)-10,15,20-triphenylporphyrin, a second-generation photosensitizer that is relatively easy to synthesize and exhibits a singlet oxygen quantum yield of $\Phi\Delta$=0.57 (Managa et al., 2016). TPPOH was covalently linked to xylan via an esterification reaction and then this conjugate was attached to SNPs through ionic bonds. The *in vitro* cytotoxicity and photodynamic efficiency of these nanomaterials were determined against HCT116 and HT-29 colorectal cancer cell lines.

2. Materials and methods

2.1. Materials

For a list of materials, see Supplementary Information (SI).

2.2. Analytical methods

FTIR analyses were performed on a Perkin Elmer FT-IR Spectrum 1000 spectrometer using KBr pellets (1-2 wt%). NMR analyses were carried out on a Bruker DPX 500 NMR spectrometer, operating at 500 MHz. UV–vis spectra were recorded on a double beam spectrophotometer AnalytikaJena SPECORD 210, using 10 mm quartz cells. High resolution electrospray ionization mass spectrometry (HR ESI-MS) was performed at the ICOA/CBM platform (Orléans University) on a Bruker Q-TOF maXis mass spectrometer, coupled to an Ultimate 3000 RSLC chain (Dionex). Purifications were performed with Combiflash Rf 100® from Teledyne Isco. The stationary phase consisted of an 80 g silica column. The products to be purified were solubilized in a minimum amount of solvent and fixed on Florisil (60-100 mesh, VWR). For Transmission Electron Microscopy (TEM) studies, one droplet of nanoparticle suspension was lyophilized on a copper grid. Images were taken with a JEOL 2010 UHR instrument. Particle size distribution and zeta potential were analyzed through dynamic light scattering (DLS) using a Zetasizer Nano-ZS (Malvern, UK). SNPs suspension was diluted in absolute ethanol and analyzed at 20 °C at a scattering angle of 173°. The mean diameter of SNPs was expressed as the average value of two measurements, each one comprising 15 runs. Zeta potential data was collected through electrophoretic light scattering at 20 °C, 150 V using this same instrument. Each zeta potential value is the average of two measurements, each one comprised of 100 single runs. Red light (630-660nm, 75 J/cm2) was delivered from the light source PhotoCureTM Lamp CURElight (PhotoCure ASA, Oslo, Norway). Cell morphology was analyzed by an electron microscope JEOL JEM-1011 operated at 80 KeV (JEOL, Croissy-sur-Seine, France).

2.3. Porphyrin synthesis

2.3.1. [3-ethoxycarbonylpropyloxy] phenyl) -10,15,20-triphenylporphyrin **(2)**

5-(4-hydroxyphenyl)-10,15,20-triphenylporphyrin (**1**) was synthesized according to the Little method (Little, Anton, Loach, & Ibers, 1975; Boscencu, Licsandru, Socoteanu, Oliveira, & Ferreira, 2007). Compound **1** (0.2 g, 1 equiv, 0.32 mmol) was dissolved in 15 mL of DMF with excess K_2CO_3 (25 equiv, 1.09 g, 7.92 mmol) and stirred for 5 min at room temperature. Then 0.43 g of ethyl 4-bromobutyrate (7 equiv, 2.22 mmol) were added. The reaction was carried out using microwave irradiation at 120 °C and 300 W for 7 min and monitored by thin-layer chromatography (TLC). After evaporation of DMF under vacuum, the crude product was dissolved in chloroform (15 mL). The organic layer was washed with water (3 ×

30 mL), dried ($MgSO_4$) and then evaporated to give, after purification by flash chromatography on a silica column, (eluent: petroleum ether/$CHCl_3$ from 80 to 100%) a pure porphyrin **2** with 91% yield. Rf= 0.44 ($CHCl_3$), ^{1}H NMR ($CDCl_3$, 500.15 MHz) δH, ppm : -2.74 (s, 2H, NH pyrrole), 1.32 (t, 3H, J = 7.5 Hz, CH_3 ethyl), 2.27 (q, 2H, J= 6.5 Hz, Hβ -CH_2-), 2.66 (t, 2H, J = 7.5 Hz, -CH_2-C=O), 4.22 (q, 2H, J= 7 Hz, CH_2 ethyl), 4.25 (t, 2H, J= 6 Hz, -O-CH_2-), 7.22 (d, 2H, J= 8.5 Hz, H3,5 aryl), 7.72 (m, 9H, H3,4,5 phenyl), 8.10 (d, 2H, J = 8.5 Hz, H2,6 aryl), 8.20 (d, 6H, J= 7.5 Hz, H2,6 phenyl), 8.83 (s, 8H, Hβ pyrrole). ^{13}C NMR ($CDCl_3$, 500.15 MHz) δc, ppm : 14.31 (CH_3 ethyl) ; 24.87 (-CH_2-) ; 30.99 (CH_2-C=O) ; 60.52 (CH_2 ethyl); 67.03 (O-CH_2); 112.72 (C-3,5 aryl); 119.96-120.07 (C meso); 126.68-127.67 (C phenyl); 130.88-131.13 (Cβ pyrrole); 134.54-134.59 (C-2,6 aryl); 135.59 (C-1 aryl) ; 142.19-142.22(Cα pyrrole); 158.70 (C-4 aryl); 173.30 (C=O). UV-Visible : UV-Vis ($CHCl_3$) λ max nm (ε, 10^3 L.mol^{-1}.cm^{-1}) : 420 (609), 519 (21), 553 (10), 591 (6), 649 (5). MS (ESI): m/z = 745.3173 [M+H] $^+$.

2.3.2. 5-(2-[3-carboxypropyloxy] phenyl) -10,15,20-triphenylporphyrin (**3**)

Compound **2** (0.3 g, 1 equiv, 0.4 mmol) was dissolved in 15 mL DMF and then 0.16 g (10 equiv, 4 mmol) NaOH previously dissolved in 2 mL of distilled water, was added. The reaction was allowed to proceed under stirring for 2 h at 100 °C. After solvent evaporation, the crude product was dissolved in chloroform (15 mL) and neutralized with 287.5 µL hydrochloric acid (HCl) (37%, 12 M), washed with distilled water (3x30 mL), dried over $MgSO_4$, and evaporated. Then, the crude product was purified by flash chromatography to give TPPOH (compound **3)** as a purple solid (yield 96%) (eluent: $CHCl_3$/Ethanol from 100 to 90%). Rf= 0.6 (EtOH/$CHCl_3$ 1/9), ^{1}H NMR ($CDCl_3$+10% TFA, 500.15 MHz) δH, ppm: 2.39 (q, 2H, -CH_2-, J= 8Hz), 2.86 (t, 2H, CH_2-C=O, J = 6.5Hz), 2.48 (t, 2H, CH_2-O, J= 6Hz), 7.56 (d, 2H, H3,5 aryl, J= 7.7Hz), 8.02 (m, 9H, H3,4,5 phenyl), 8.53 (m, 8H, H2,6 phenyl, H2,6 aryl), 8.7 (s, 8H, Hβ pyrrole). ^{13}C NMR ($CDCl_3$, 500.15 MHz) δc, ppm : 24.6 (-CH_2-) ; 30.9 (CH_2-C=O) ; 67.1 (O-CH_2); 115.09 (C-3,5 aryl); 122.44-123.98 (C meso) ; 128.79-129.55 (C phenyl) ; 130.79-133.02 (C βpyrrole) ; 139.2-138.3 (C-2,6 aryl); 140.3 (C1 aryl) ; 146.46-145.17(C αpyrrole) ; 161.1 (C-4 aryl) ; 181 (C=O). UV-Vis ($CHCl_3$) λ max nm (ε, 10^3 L.mol^{-1}.cm^{-1}): 420 (451), 516 (21), 553 (10), 591 (6), 647 (5). MS (ESI): m/z = 717.286 [M+H] $^+$.

2.4. Synthesis of PX

3.4.1. Solubilization of xylan

Xylan (1g) was dissolved in 20 mL DMSO (60 °C) and filtered to remove the insoluble fraction. To determine the concentration of this solution, 1 mL was precipitated with 3 mL absolute ethanol, filtered and dried under vacuum. The mass of precipitated xylan was 44.5 mg, therefore the xylan solution in DMSO had a concentration of 44.5 mg/mL (absence of polysaccharide in the filtrate was verified by TLC.

3.4.2. TPPOH grafting to xylan

All syntheses were carried out following the same protocol. TPPOH was added to 1 equivalent of N, N-carbonyldiimidazole (CDI) and stirred in DMSO at room temperature for 24 h. This solution was then added to a solution of 100 mg (0.76 mmol anhydroxylose unit) xylan in DMSO and allowed to react under stirring. Reaction parameters are summarized in Table S1 (SI). The product was precipitated out in absolute ethanol and was washed three times with ethanol and three times with chloroform to remove unreacted starting material and then dried under vacuum.

2.5. Synthesis and surface modification of SNPs

3 mL aqueous ammonia (28%) and 1.5 mL tetraethoxysilane (TEOS) were successively added dropwise to 45 mL absolute ethanol. This solution was stirred for 4 h at 48 °C. Resulting SNPs were collected by centrifugation (8000 rpm, 30 min), washed three times with ethanol and then dispersed in 25 mL 96% ethanol. Then, 4 mL (3-aminopropyl) triethoxysilane (APTES) was added and stirred overnight. After three cycles of centrifugation/redispersion in ethanol, SNPs were obtained as a white solid and were stored in 25 mL of absolute ethanol.

2.6. Grafting of PX onto surface-modified SNPs

PX (10 mg) was dissolved in 20 mL distilled water. Then 100 mg SNPs in ethanol were added dropwise and ultrasonicated during the addition. This mixture was then stirred for 20 min. The resulting PX SNPs were centrifuged and washed three times with water and absolute ethanol.

226 2.7. Determination of TPPOH concentration in SNPs

227 The amount of TPPOH attached to the SNPs was determined by UV-visible assay. PX SNPs
228 were dispersed in absolute ethanol at a concentration of 10 mg/mL and diluted to 0.5 mg/mL.
229 Absorbance of this sample was measured at 418 nm, and absorbance of SNPs was subtracted.
230 The PX content of SNPs was calculated from a calibration curve constructed with different
231 concentrations of free PX in distilled water. The concentration of TPPOH in mol/L was
232 calculated according to Eq. (1):

$$C = \frac{DSxM(PX)}{M(repeat\ unit\ of xylan) + DSx(M(TPPOH) - 18)} \quad (1)$$

233 M(PX) = concentration of PX in g/L attached to SNPs, calculated from the standard
234 calibration curve

235 M (repeat unit of xylan: xyl/MeGlcA 10 :1) = 1511 g/mol

236 M (TPPOH)= 717.286 g/mol

237 2.8. In vitro experiments

238 2.8.1. Cell lines, cell culture, and PX SNPs

239 For all experiments, cells were seeded at $1.2x10^4$ cells/cm^2 and $2.08x10^4$ cells/cm^2 for
240 HCT116 and HT-29 cells, respectively and were grown for 24 h in culture medium prior to
241 exposure, or lack of, to TPPOH or PX SNPs at indicated concentrations. Stock solutions of
242 TPPOH (5 mg/mL) and PX SNPs 80 nm (20 mg/mL) were prepared in ethanol.

243 2.8.2. PX SNPs toxicity tests

244 PX-SNPs cytotoxicity was determined using 3-(4,5-dimethylthiazol-2-yl)-2,5-
245 diphenyltetrazolium bromide (MTT) assays. Human colorectal cancer cells were seeded at
246 $4x10^3$ cells/well and $7x10^3$ cells/well for HCT116 and HT-29 cells, respectively, in 96-well
247 culture plates and grown for 24 h in culture medium prior to exposure, or lack of, to TPPOH
248 or PX SNPs. Stock solutions of TPPOH and PX SNPs were diluted in culture medium to
249 obtain the appropriate final concentrations. The same amount of vehicle (percentage of
250 ethanol did not exceed 0.6%) was added to control cells. After 24 h, culture medium was
251 replaced by phenol red-free culture medium and cells were irradiated, or not, by red light
252 (630-660 nm, 75 J/cm^2). MTT assays were done 48 h after irradiation and experiments were
253 performed in triplicate.

2.8.3. Transmission electron microscopy (TEM)

HCT116 cells ($3x10^5$) were seeded in 25 cm^2 tissue culture flasks and grown for 24 h in culture medium prior to exposure or not to PX SNPs. After 24 h, culture medium was replaced by phenol red-free culture medium and cells were irradiated, or not, by red light (75 J/cm²). Then, cells were fixed in 2.5% glutaraldehyde for 30 min at room temperature and washed in phosphate buffer for 15 min. They were then incubated in 1% osmium tetroxide solution for 30 min at room temperature, dehydrated with increasing ethanol concentrations, and embedded in epon. They were polymerized over 48 h at 60 °C and ultrathin sections (80-100 nm) were prepared. Grids were stained with uranyl acetate and lead citrate and examined with TEM operated at 80 KeV.

2.8.4. Statistical analysis

Data are expressed as the arithmetic means ± standard error of the mean (SEM) of separate experiments. The statistical significance of results obtained from *in vitro* studies was evaluated by the two tailed unpaired Student's t-test, with $p<0.05$ being considered as significant.

3. Results and discussion

Preparation of PX SNPs is summarized in Fig.1. TPPOH was conjugated with xylan via an esterification reaction forming PX which was used in the surface modification of SNPs. The presence of glucuronic acid groups on xylan allows the formation of ionic bonds on the surface of SNPs which is made cationic by APTES.

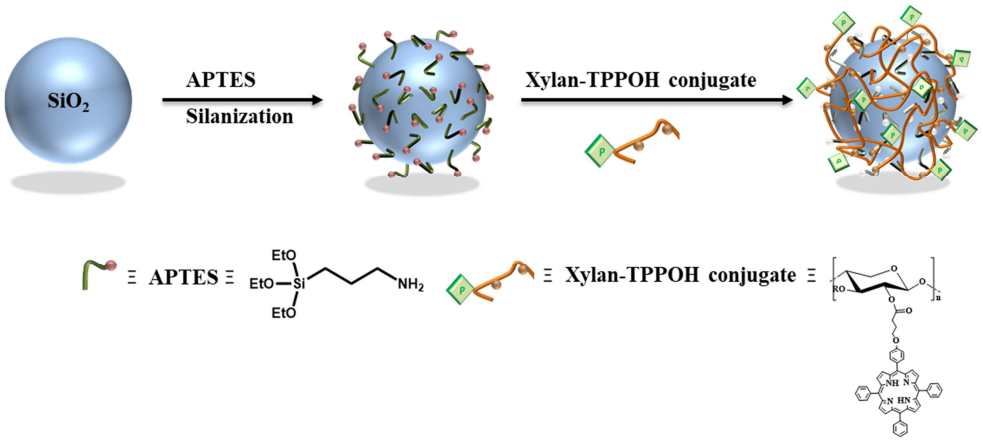

Fig. 1. General procedure for the synthesis of PX SNPs.

3.1. Characterization of xylan

The xylan used in this study was characterized by the classical methods already described in the literature (Kerrouche et al. 2018). It had an average polymerization degree of 208 calculated as the ratio of amount of total sugars to the quantity of reducing sugars. The composition was characterized by colorimetric assay and contained 92.5% xylose and 7.5% glucuronic acids. ^{1}H NMR spectrum of this xylan (Fig. S1, SI) showed the signal corresponding to anomeric protons of substituted xylose units at 4.5 ppm, non-substituted xylose units at 4.6 ppm and anomeric protons of uronic acid at 5.3 ppm. The degree of substitution of xylan by 4-*O*-methylglucuronic acid, which was about 1/10, was calculated according to Eq. (A.1, SI).

3.2. PX synthesis

The synthesis route of PX is summarized in Fig. 2. First, 5-(4-hydroxyphenyl)-10,15,20-triphenylporphyrin **(1)** was synthesized according to the Little method and obtained with a 3.7% yield in agreement with the literature. It was then functionalized with ethyl 4-bromobutyrate through nucleophilic substitution, activated by microwave irradiation according to Chaleix et al. (2009). Product **2** was obtained with 91% yield. After saponification with sodium hydroxide, porphyrin derivative **3** was obtained with 96% yield. The structures of all compounds were confirmed by ^{1}H, ^{13}C NMR and mass spectrometry. Compound **3** was then covalently attached to xylan by esterification using CDI as the coupling reagent.

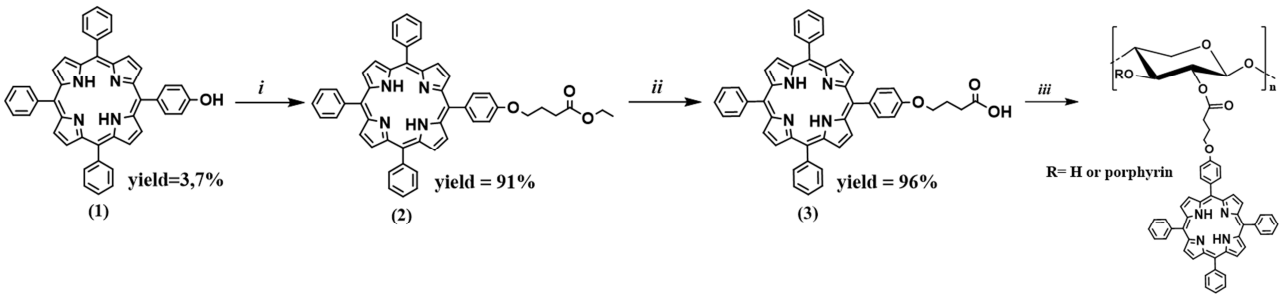

Fig. 2. Synthesis of PX. *i*: ethyl 4-bromobutyrate, K_2CO_3, DMF, MW; *ii*: NaOH, DMF/Water, HCl (0.1M); *iii*: Xylan, DMSO, CDI, t(h), T(°C).

The covalent binding between xylan and TPPOH was confirmed by FTIR. The corresponding FTIR spectrum of PX is displayed in Fig. 3 (c). This compound and native xylan (Fig. 3 b),

shared a characteristic absorption band around 3400 cm^{-1}, which has been assigned to the stretching vibrations of hydroxyl groups of xylan. There were two other bands at 2920 cm^{-1} and 1441 cm^{-1} that represent the stretching and deformation vibrations of C-H bond. PX also displayed new signals that correspond to the TPPOH moiety (1245, 1178, 796, 730 cm^{-1}) and a peak at 1739 cm^{-1} that corresponds to the carbonyl functionality of TPPOH. The ^{1}H NMR spectrum of modified xylan (Fig. 4) identified protons of the xylose units between 3 and 5.5 ppm, and the peripheral protons of TPPOH between 7 and 9 ppm. The broad singlet at -2.9 ppm was assigned to the NH internal protons of the porphyrin pyrrole units, which is in agreement with classical ^{1}H NMR spectra of porphyrins.

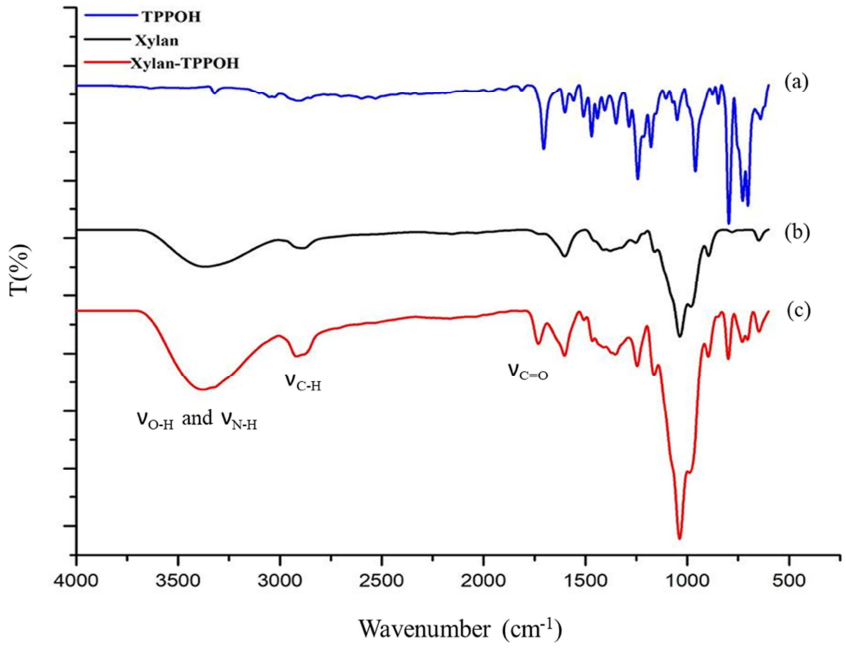

Fig. 3. FTIR Spectra of TPPOH (a), native xylan (b), and PX (c).

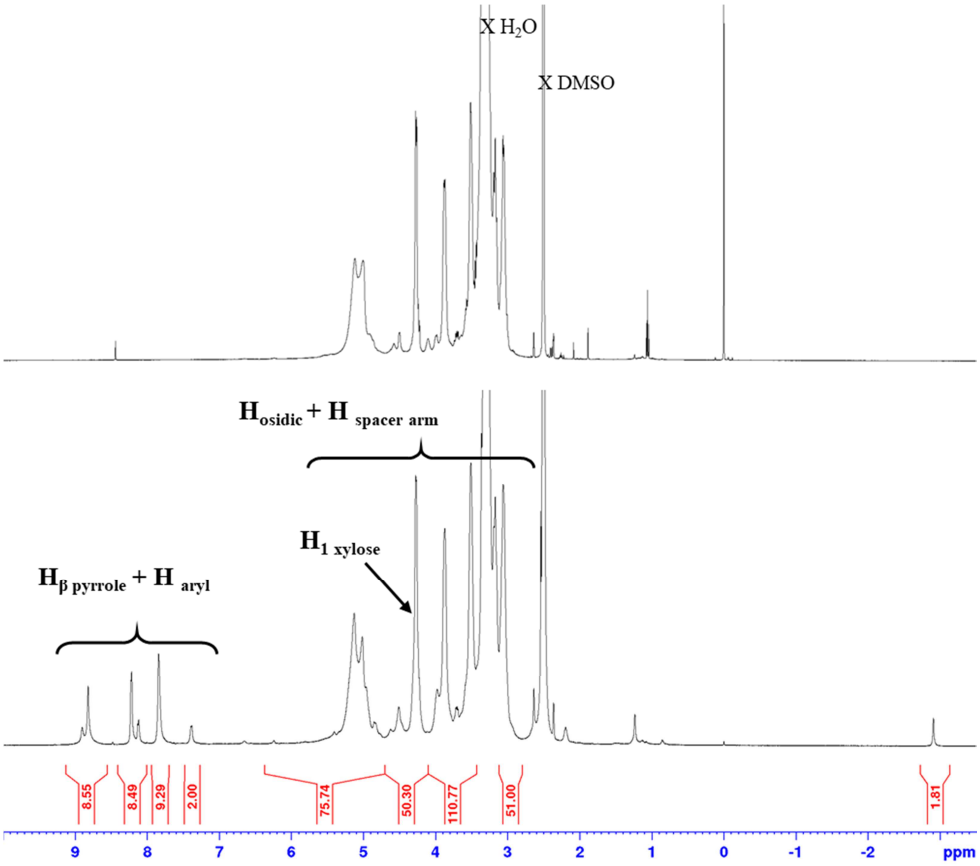

Fig. 4. ^{1}H NMR spectra of native xylan (a), and PX (b) in DMSO (DS=0.2).

3.3. Experimental design

Esterification reactions are mainly influenced by reaction time, temperature and molar ratio of reagents. The efficiency of this esterification reaction was expressed by the degree of substitution and weight yield. In order to determine optimal conditions and study the variations of the degree of substitution (DS) and weight yield as a function of temperature, reaction time and TPPOH equivalents, an experimental design was built. The choice of factors and their modes are listed in Table S2 (SI). For 3 factors, 27 experiments needed to be performed to explore the entire experimental field. In order to reduce the number of tests and still keep the possibility of studying all factors, a latin square design of experiments was constructed. In this way only nine experiments were performed, applying the experimental conditions summarized in Table S1 (SI). For the nine samples, DS and weight yield were measured and the obtained values listed in Table S3 (SI).

DS was expressed as the number of TPPOH molecules per xylan repeat unit. The DS value was calculated from ^{1}H NMR data according to Eq. (2):

$$DS = \frac{H(TPPOH)/27}{H1(xylan)/10} \quad (2)$$

Where H(TPPOH) is the integral area of TPPOH protons at δ 7.26-9.12 ppm, and H1(xylan) is the integral area of anomeric protons of substituted and non-substituted xylose units at δ 4.12-4.7 ppm. To determine the effect of each factor on the degree of substitution in TPPOH, independently from the other factors, an average DS for each modality was calculated. Then, variation of the mean DS according to the modalities of the three factors was examined. As shown in Fig. 5, at all temperature and reaction times, an increase in TPPOH equivalents led to an increase in DS. Reaction time had no significant effect on DS beyond 24 hours. Furthermore, temperature increases over 50°C resulted in a drop in DS.

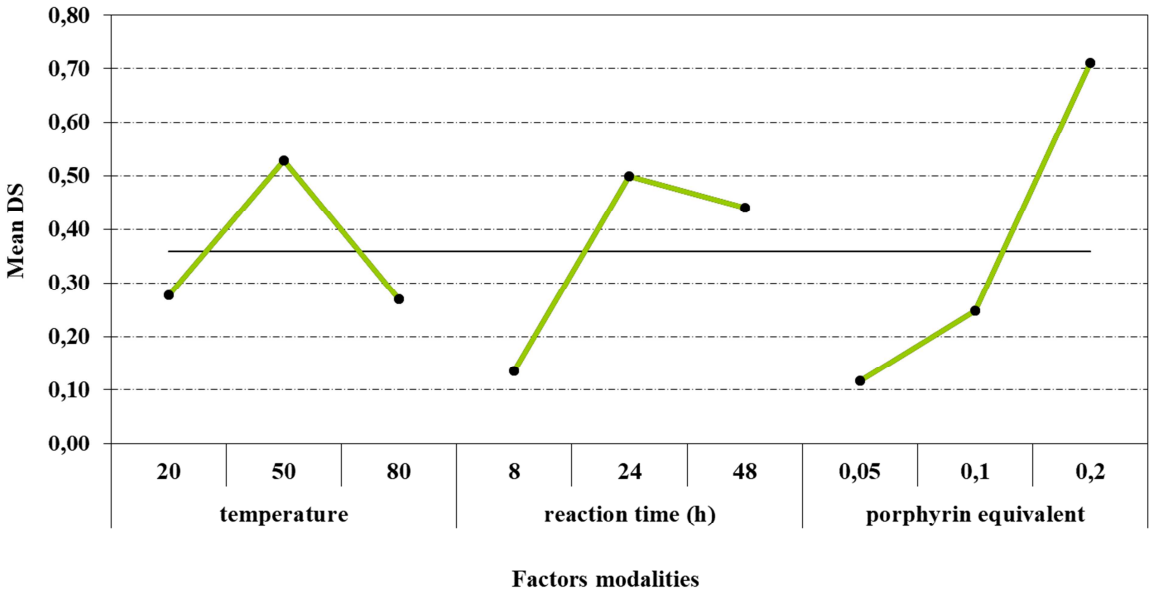

Fig. 5. Average effect of temperature, reaction time and TPPOH equivalent on DS.

The influence of these factors on weight gain was also studied. The variation of the average weight yield according to each factor is illustrated in Fig. 6.

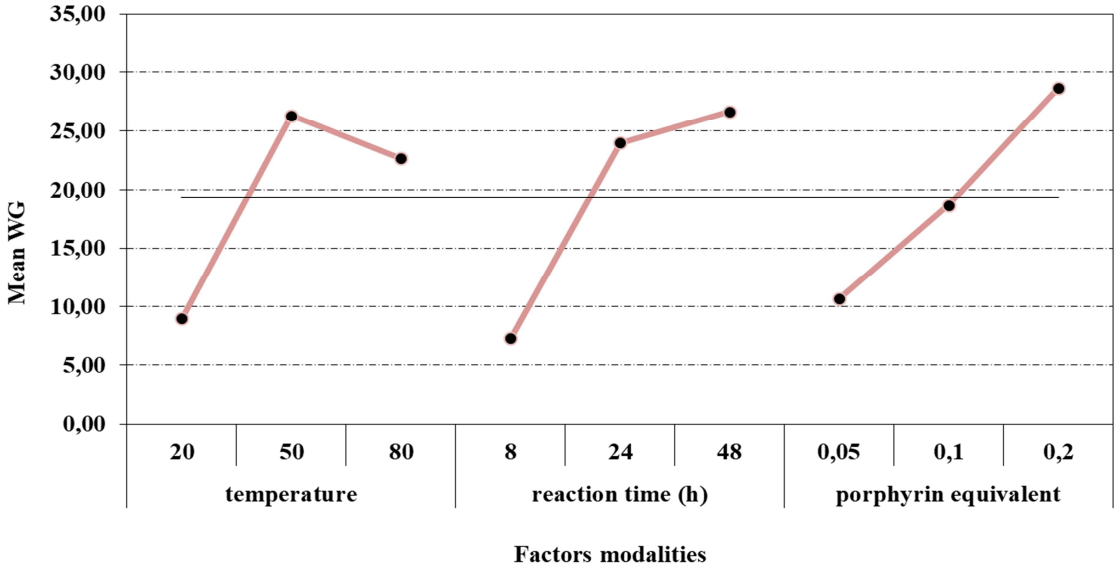

Fig. 6. Effects of temperature, reaction time and TPPOH equivalent on weight yield.

Increases in the amount of TPPOH led to increased weight yields, and a slight increase in weight was observed as a function of reaction time beyond 24 h. Temperatures above 50 °C induced a slight decrease in DS.

Different degrees of substitution ranging from 0.034 to 1.11 were obtained. Among the nine samples we chose S9 sample showed the highest DS in TPPOH (DS = 0.2) while remaining water soluble.

3.4. Synthesis of core-shell hybrid nanoparticles

3.4.1. Synthesis of SNPs

To prepare core-shell hybrid nanoparticles, SNPs were first synthesized by the sol-gel process based on the modified Stöber method (Stöber, Fink, & Bohn, 1968), using TEOS as starting material. Monodispersed colloidal silica particles were produced by hydrolysis and polycondensation of TEOS, in the presence of ammonia as a catalyst in alcoholic media.

TEM images showed spherical shape nanoparticles with an average diameter of 80 nm (Fig. 7 A). Dynamic light scattering (DLS) confirmed TEM results and the hydrodynamic diameter was measured as 78.43±19.92 nm with a 0.062 polydispersity index (PDI). Zeta potential measurements showed the presence of negative charges on the surface of nanoparticles due to hydroxyl groups, as reported in Table S4 (SI).

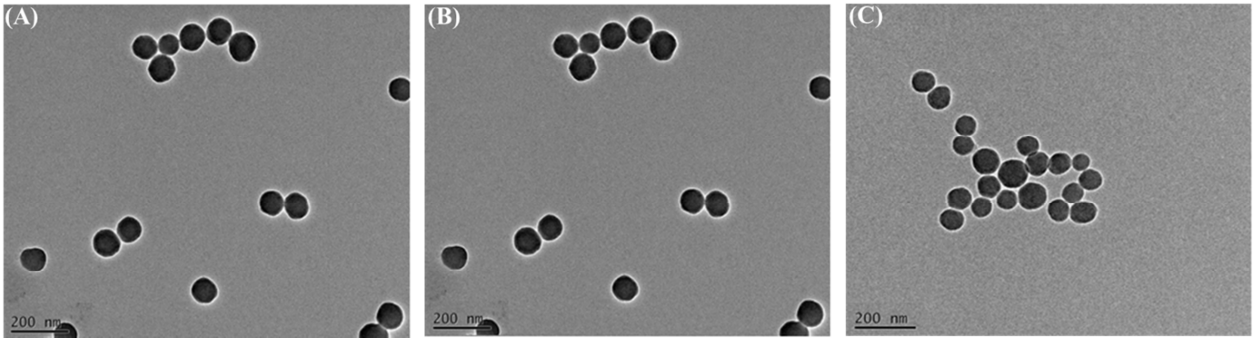

Fig. 7. TEM images of (A) SNPs, (B) SNPs-APTES, and (C) PX SNPs.

These nanoparticles were then functionalized by APTES according to the same sol-gel mechanism. The surface modification of SNPs was confirmed by zeta potential measurements. Results showed the presence of positive charges on the surface of nanoparticles due to the ammonium groups supplied by APTES. TEM measurements (Fig. 7 B) showed no significant changes in size compared to starting nanoparticles. DLS size distribution and zeta potential curves are reported in Fig. S2 (SI).

3.4.2. Functionalization of SNPs with PX

Beech xylan exhibits a specific xylose to methyl-glucuronic acid ratio estimated to be 10:1. Furthermore, it has been reported that the pKa value for the most common types of uronic acids found in xylan is 3.2–3.7 (Österberg, Laine, Stenius, Kumpulainen, & Claesson, 2001). Therefore, in ultra-pure water (pH~6.5) glucuronic acid groups will allow the attachment of xylan to the SNPs through ionic bonds with the previously introduced ammonium groups. In practice, a suspension of SNPs in ethanol was added dropwise to a solution of PX in water. The resulted PX SNPs were collected by centrifugation and the unattached polymer was removed by washing several times with water. Color change of SNPs after coating with PX can be seen in Fig. S3 (SI). TEM measurements (Fig. 7 C) showed no significant changes in size and shape of SNPs.

The functionalization of SNPs with PX was confirmed by UV-visible analysis (Fig. S4, SI). The amount of PX bound to the nanoparticles was evaluated using a standard calibration curve obtained from different concentrations of free PX diluted in water. We used a PX characterized by a 0.2 degree of substitution which associated 9.77×10^{-6} mol TPPOH per gram of silica (Table S5, SI).

3.5. In vitro cytotoxicity of PX SNPs

Phototoxicity of TPPOH and PX SNPs was studied in two human colorectal cancer cell lines with different grade: HCT116 (grade I) and HT-29 (grade II). Toxicity was determined 48 h post-irradiation by MTT assay. Both compounds proved to be non toxic against cells kept in the dark (data not shown). When the PS was irradiated by 630-660 nm red light, strong toxicity was exerted on the cell lines. IC_{50} values were determined (Table 1) in order to compare PS effects. We observed that TPPOH was less effective against the two human colorectal cancer cell lines. In fact, compared to TPPOH, PX SNPs were 40-fold and 10-fold more effective against HCT116 cells against HT-29 cells respectively, the former being significantly less resistant than the latter. These compounds were used at their respective IC_{50} values in the next experiments.

Table 1. *In vitro* phototoxicity of PX SNPs in human colorectal cancer cells.

	IC_{50} (nM)	
	HCT116	HT-29
TPPOH free	2943 ± 102	5959 ± 430
PX SNPs [a]	72.6 ± 2.8	550.2 ± 7.5

[a] IC50 nM concentrations are directly corresponding to the amount of TPPOH on the SNPs.

The morphology of HCT116 cells was characterized by TEM analysis (Fig. 8). After 630-660 nm irradiation, untreated cells exhibited abundant microvilli, the sign of normal morphology. Cells treated with PX SNPs kept in the dark showed NPs uptake without morphological changes. However, cells treated with PX SNPs and then irradiated showed complete breakdown of intracellular structures. These cells exhibited morphological features such as cell membrane shrinkage, nuclear condensation and formation of phagocytic vesicles or apoptotic bodies, hallmark events of apoptotsis (Elmore, 2007).

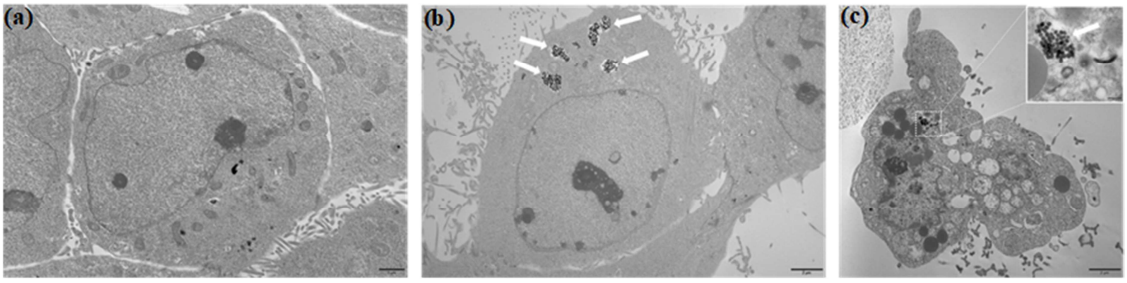

Fig. 8. TEM analysis of HCT116 cells (a) control cell (irradiated) (b) PX SNPs (dark), (c) PX SNPs (irradiated); White arrows indicate SNPs inside cytoplasm.

4. Conclusion

Xylan was successfully modified with TPPOH and nine samples were obtained with DS ranging from 0.034 to 1.11. The sample showing the highest DS in TPPOH while remaining soluble in water was used to coat SNPs through ionic bonds. The color change of SNPs even after several washes with distilled water indicated efficient coating of SNPs with PX. Thus, xylan proved effective for the surface incorporation of active molecules in controlled quantities. At the cellular level, the conjugation of TPPOH to SNPs significantly enhanced its solubility and consequently its uptake by cancer cells. Therefore, the cell-killing efficiency

was higher with PX SNPs compared to free TPPOH. Furthermore, cell death occurred by apoptosis as confirmed by TEM morphological characterization.

Acknowledgments

The authors are indebted to Dr. Michel Guilloton, Dáire Gibbons, and Jeanne Moreau for help in manuscript editing, and they gratefully acknowledge Pierre Carles (Carmalim Plateform-IRCER– University of Limoges) for TEM images and Dr. Yves Champavier for NMR analysis.

References

Abrahamse, H., & Hamblin, M.R. (2016). New photosensitizers for photodynamic therapy. *Biochemical Journal*, 473, 347–364.

Bonnett, R. (1995). Photosensitizers of the porphyrin and phthalocyanine series for photodynamic therapy. *Chemical Society Reviews*, 24, 19–33.

Boscencu, R., Licsandru, D., Socoteanu, R., Oliveira, A.S.,Ferreira, L.F.V. (2007). Synthesis and spectral characterization of some unsymmetrically-substituted mesoporphyrinic compounds. *Revista de Chimie*, 58, 498–501.

Bharathiraja, S., Moorthy, M.S., Manivasagan, P., Seo, H., Lee, K.D., & Oh, J. (2017). Chlorin e6 conjugated silica nanoparticles for targeted and effective photodynamic therapy. *Photodiagnosis and Photodynamic Therapy*, 19, 212–220.

Brezániová, I., Záruba, K., Králová, J., Sinica, A., Adámková, H., Ulbrich, P., Poučková, P., Hrubý, M., Štěpánek, P., & Král, V. (2018). Silica-based nanoparticles are efficient delivery systems for temoporfin. *Photodiagnosis and Photodynamic Therapy*, 21, 275–284.

Coombes, A.G.A., Tasker, S., Lindblad, M., Holmgren, J., Hoste, K., Toncheva, V., Schacht, E., Davies, M.C., Illum, L., & Davis, S.S. (1997). Biodegradable polymeric microparticles for drug delivery and vaccine formulation: the surface attachment of hydrophilic species using the concept of poly (ethylene glycol) anchoring segments. *Biomaterials*, 18, 1153–1161.

Chaleix, V., Couleaud, P., Sol, V., Zerrouki, R., Alves, S., & Krausz, P. (2009). Microwave-assisted expeditious O-alkylation of *meso*-hydroxyphenylporphyrins. *Journal of Porphyrins and Phthalocyanines*, 13, 888–892.

449 Daus, S., & Heinze, T. (2010). Xylan-based nanoparticles: prodrugs for ibuprofen release.
450 *Macromolecular Bioscience*, 10, 211–220.

451 Drogat, N., Granet, R., Le Morvan, C., Bégaud-Grimaud, G., Krausz, P., Sol, V. (2012).
452 Chlorin-PEI-labeled cellulose nanocrystals: synthesis, characterization and potential
453 application in PDT. *Bioorganic & Medicinal Chemistry Letters*, 22, 3648–3652.

454 Debele, T.A., Peng, S., & Tsai, H.C. (2015). Drug carrier for photodynamic cancer therapy.
455 *International Journal of Molecular Sciences*, 16, 22094–22136.

456 Ebringerová, A., Hromádková, Z., & Heinz, T. (2005). Hemicellulose. *Advances in Polymer*
457 *Science*, 186, 1–67.

458 Elmore, S. (2007). Apoptosis: a review of programmed cell death. *Toxicologic Pathology*, 35,
459 495–516.

460 Frank, M.M., & Fries, L.F. (1991). The role of complement in inflammation and
461 phagocytosis. *Immunology Today*, 12, 322–326.

462 Gref, R., Minamitake, Y., Peracchia, M.T., Trubetskoy, V., Torchilin, V., & Langer, R.
463 (1994). Biodegradable long-circulating polymeric nanospheres. *Science*, 263, 1600–1603.

464 Henderson, B.W., & Dougherty, T.J. (1992). How does photodynamic therapy work?
465 *Photochemistry and photobiology*, 55, 145–157.

466 Kerrouche, Dj., Sadoun, T., Stoclet, G., Sol, V., Gloaguen, V., Chaleix, V. (2018) Synthesis
467 and characterization of xylan-graft-poly(L-lactide). *International Journal of Polymer Analysis*
468 *and Characterization*, 23, 193-206

469 Kydd, J., Jadia, R., Velpurisiva, P., Gad, A., Paliwal, S., & Rai, P. (2017). Targeting
470 strategies for the combination treatment of cancer using drug delivery systems.
471 *Pharmaceutics*, 9, 46.

472 Kwiatkowski, S., Knap, B., Przystupski, D., Saczko, J., Kędzierska, E., Knap-Czop, K.,
473 Kotlińska, J., Michel, O., Kotowski, K., & Kulbacka, J. (2018). Photodynamic therapy–
474 mechanisms, photosensitizers and combinations. *Biomedicine & Pharmacotherapy*, 106,
475 1098–1107.

476 Little, R.G., Anton, J.A., Loach, P.A., & Ibers, J.A. (1975). The synthesis of some substituted
477 tetraarylporphyrins. *Journal of Heterocyclic Chemistry*, 12, 343–349.

Lemarchand, C., Gref, R., & Couvreur, P. (2004). Polysaccharide-decorated nanoparticles. *European Journal of Pharmaceutics and Biopharmaceutics*, 58, 327–341.

Matsumura, Y., & Maeda, H. (1986). A new concept for macromolecular therapeutics in cancer chemotherapy: mechanism of tumoritropic accumulation of proteins and the antitumor agent smancs. *Cancer Research*, 46, 6387–6392.

Maeda, H., & Matsumura, Y. (1989). Tumoritropic and lymphotropic principles of macromolecular drugs. *Critical Reviews in Therapeutic Drug Carrier Systems*, 6, 193–210.

Maeda, H. (2001). The enhanced permeability and retention (EPR) effect in tumor vasculature: the key role of tumor-selective macromolecular drug targeting. *Advances in Enzyme Regulation*, 41, 189–207.

Moine, C., Krausz, P., Chaleix, V., Sainte-Catherine, O., Kraemer, M., & Gloaguen, V. (2007). Structural characterization and cytotoxic properties of a 4-O-methylglucuronoxylan from castanea sativa. *Journal of Natural Products*, 70, 60–66.

Melo-Silveira, R.F., Fidelis, G.P., Pereira Costa, M.S.S., Silva Telles, C.B., Dantas-Santos, N., de Oliveira Elias, S., Bley Ribeiro, V., Barth, A. L., Macedo, A. J., Lisboa Leite, E., & Oliveira Rocha, H. A. (2012). *In vitro* antioxidant, anticoagulant and antimicrobial activity and in inhibition of cancer cell proliferation by xylan extracted from corn cobs. *International Journal of Molecular Sciences*,13, 409–426.

Managa, M., Mack, J., Gonzalez-Lucasb, D., Remiro-Buenamañana, S., Tshangana, C., Cammidge, A.N., Nyokong, T. (2016). Photophysical properties of tetraphenylporphyrinsubphthalocyanine conjugates. *Journal of Porphyrins and Phtalocyanines*, 20, 1–20.

Mbakidi, J-P., Herke, K., Alvès, S., Chaleix, V., Granet, R., Krausz, P., Leroy-Lhez, S., Ouk, T-S., Sol, V. (2013). Synthesis and photobiocidal properties of cationic porphyrin-grafted paper. *Carbohydrate Polymers*, 99, 333-338.

Ma, J., Li, D., Zhong, L., Du, F., Tan, J., Yang, J., & Peng, X. (2018). Synthesis and characterization of biofunctional quaternized xylan-Fe2O3 core/shell nanocomposites and modification with polylysine and folic acid. *Carbohydrate Polymers*, 199, 382–389.

Mozar, F.S., & Chowdhury, E.H. (2018). PEGylation of carbonate apatite nanoparticles prevents opsonin binding and enhances tumor accumulation of gemcitabine. *Journal of Pharmaceutical Sciences*, 107, 2497–2508.

Nagai, H., & Kim, Y.H. (2017). Cancer prevention from the perspective of global cancer burden patterns. *Journal of Thoracic Disease*, 9, 448–451.

Österberg, M., Laine, J., Stenius, P., Kumpulainen, A., & Claesson, P.M. (2001). Forces between xylan-coated surfaces: effect of polymer charge density and background electrolyte. *Journal of Colloid and Interface Science*, 242, 59–66.

Owens D.E. 3rd, & Peppas N.A. (2005). Opsonization, biodistribution, and pharmacokinetics of polymeric nanoparticles. *International Journal of Pharmaceutics*, 307, 93–102.

Peracchia, M.T., Fattal, E., Desmaële, D., Besnard, M., Noël, J.P., Gomis, J.M., Appel, M., d'Angelo, J., & Couvreur, P. (1999). Stealth PEGylated polycyanoacrylate nanoparticles for intravenous administration and splenic targeting. *Journal of Controlled Release*, 60, 121–128.

Roy, I., Ohulchanskyy, T.Y., Pudavar, H.E., Bergey, E.J., Oseroff, A.R., Morgan, J., Dougherty, T.J., & Prasad, P.N. (2003). Ceramic-based nanoparticles entrapping water-insoluble photosensitizing anticancer drugs: a novel drug-carrier system for photodynamic therapy. *Journal of the American Chemical Society*, 125, 7860–7865.

Ringot, C., Saad, N., Brégier, F., Bressollier, P., Poli, E., Chaleix, V., Ouk, T.S., Sol, V. (2018). Antibacterial activity of a photosensitive hybrid cellulose fabric. *Photochemical and Photobiological Sciences*, 17, 1780–1786.

Stöber, W., Fink, A., & Bohn, E. (1968). Controlled growth of monodisperse silica spheres in the micron size range. *Journal of Colloid and Interface Science*, 26, 62–69.

Sternberg, E.D., Dolphin, D., & Brückner, C. (1998). Porphyrin-based photosensitizers for use in photodynamic therapy. *Tetrahedron*, 54, 4151–4202.

Saini, R.K., Chouhan, R., Bagri L.P. & Bajpai, A.K. (2012). Strategies of targeting tumors and cancers, *Journal of Cancer Research Updates*, 1, 129–152.

Tamba, B.I., Dondas, A., Leon, M., Neagu, A.N., Dodi, G., Stefanescu, C., & Tijani, A. (2015). Silica nanoparticles: preparation, characterization and in vitro/in vivo biodistribution studies. *European Journal of Pharmaceutical Sciences*, 71, 46–55.

Yan, F., & Kopelman, R. (2003). The embedding of meta-tetra(hydroxyphenyl)-chlorin into silica nanoparticle platforms for photodynamic therapy and their singlet oxygen production and pH-dependent optical properties. *Photochemistry and Photobiology*, 78, 587–591.

538 Yan, T., Cheng, J., Liu, Z., Cheng, F., Wei, X., & He, J. (2017). pH-sensitive mesoporous
539 silica nanoparticles for chemo-photodynamic combination therapy. *Colloids and Surfaces B.*
540 *Biointerfaces*, 161, 442–448.

541 Zhu, A., Yuan, L., Jin, W., Dai, S., Wang, Q., Xue, Z., & Qin, A. (2009). Polysaccharide
542 surface modified Fe3O4 nanoparticles for camptothecin loading and release. *Acta*
543 *Biomaterialia*, 5, 1489–1498.